Krzesińska, A. M., Wirth, R., Kusiak, M. (2019): Petrogenesis of ungrouped enstatite meteorite Zakłodzie: Fabric, texture, and nanostructure analysis for identification of mechanisms responsible for chondrite–achondrite transition. - *Meteoritics and Planetary Science*, *54*, 7, pp. 1462—1477.

DOI: http://doi.org/10.1111/maps.13296

The Meteoritical Society

Meteoritics & Planetary Science 54, Nr 7, 1462–1477 (2019)
doi: 10.1111/maps.13296

Petrogenesis of ungrouped enstatite meteorite Zakłodzie: Fabric, texture, and nanostructure analysis for identification of mechanisms responsible for chondrite–achondrite transition

Agata M. KRZESIŃSKA[1,2*], Richard WIRTH[3], and Monika A. KUSIAK[3,4]

[1]Centre for Earth Evolution and Dynamics, Department of Geosciences, University of Oslo, Oslo, Norway
[2]Department of Earth Sciences, Natural History Museum, Cromwell Road, SW7 5BD London, UK
[3]GeoForschungsZentrum Potsdam, Section 3.5 Surface Geochemistry, D-14473 Potsdam, Germany
[4]Institute of Geological Sciences Polish Academy of Sciences, ING PAN, Twarda 51/55, PL-00818 Warszawa, Poland
[*]Corresponding author. E-mail: a.m.krzesinska@geo.uio.no

(Received 21 June 2018; revision accepted 23 March 2019)

Abstract–Zakłodzie is an enstatite meteorite of unknown petrogenesis. Chemically, it resembles enstatite chondrites, but displays an achondrite-like texture. Here we report on fabric and texture analyses of Zakłodzie utilizing X-ray computed tomography and scanning electron microscopy and combine it with a nanostructural study of striated pyroxene by transmission electron microscopy. With this approach we identify mechanisms that led to formation of the texture and address the petrogenesis of the rock. Zakłodzie experienced a shock event in its early evolution while located at some depth inside a warm parent body. Shock-related strain inverted pyroxene to the observed mixture of intercalated orthorhombic and monoclinic polymorphs. The heat that dissipated after the peak shock was added to primary, radiogenic-derived heat and led to a prolonged thermal event. This caused local, equilibrium-based partial melting of plagioclase and metal-sulfide. Partial melting was followed by two-stage cooling. The first phase of annealing (above 500 °C) allowed for crystallization of plagioclase and for textural equilibration of metal and sulfides with silicates. Below 500 °C, cooling was faster and more heterogeneous at cm scale, allowing retention of keilite and quenching of K-rich feldspathic glass in some parts. Our study indicates that Zakłodzie is neither an impact melt rock nor a primitive achondrite, as suggested in former studies. An impact melt origin is excluded because enstatite in Zakłodzie was never completely melted and partial melting occurred during equilibrium-based postshock conditions. Texturally, the rock represents a transition of chondrite and achondrite and was formed when early impact heat was added to internal radiogenic heat.

INTRODUCTION

Enstatite meteorites represent a diverse group of highly reduced rocks, where both chondritic and achondritic rocks (aubrites) are common (Mason 1966; Brett and Keil 1986; Keil 1989, 2010). Additionally, there are a number of rocks that reveal reduced mineralogy and clear chemical affinity with enstatite chondrites but show achondritic-like textures. These meteorites, Abee, Ilafegh 009, QUE 94204, Yamato-8404, Itqiy, Happy Canyon, Zakłodzie, NWA 4301, NWA 10519, NWA 2526 are classified as ungrouped enstatite meteorites.

Although various scenarios of formation are proposed to explain petrogenesis of these ungrouped rocks, there is no consensus achieved so far. Based on the general chemical affinity to enstatite chondrites, they were proposed to represent type 7 chondrites (Stępniewski et al. 2000). However, noble gas signatures suggest that they are rather primitive achondrites that formed as residue after partial melting (Patzer et al. 2002; Keil and Bischoff 2008) or recrystallized partial or complete melts (Olsen et al. 1977; Przylibski et al. 2005). Currently, the most widely accepted interpretation is that these rocks were formed by

crystallization of impact melt and therefore represent impact melt rocks or impact melt breccias (McCoy et al. 1995; Leroux et al. 1997; Rubin and Scott 1997; Keil 2007; Udry et al. 2019). None of the scenarios, however, offers full, unequivocal explanation of how the texture was created and, as a consequence, what is the petrogenesis of these rocks.

Ambiguities regarding the petrogenesis of ungrouped enstatite meteorites are mostly caused by the fact that the achondritic-like texture they exhibit may be formed by both magmatic and metamorphic processes as well as in the course of dynamic impact melting. It is difficult to decipher magmatic and metamorphic events because various processes can take different evolutionary paths and still manifest a similar texture in the rock (e.g., Passchier and Trouw 2005). Therefore, in order to identify the exact processes related to the evolution of rocks, it is important to eliminate and strengthen the role of the exact mechanisms that were operating. The mechanisms are, in most cases, recorded in petrofabric (e.g., distribution of minerals), textural relationships of minerals (e.g., grain size distribution), and nanostructure (e.g., intracrystalline deformations). In the specific case of meteorites, the static metamorphism during accretion and impact-related processes operate under extremely different conditions; therefore, the mechanisms are usually well recorded in the highly contrasting textural relationships (e.g., Tomkins 2009; Tait et al. 2014; Guignard and Toplis 2015; Krzesińska 2017), fabric intensities (e.g., Gattacceca et al. 2005; Friedrich 2008; Krzesińska et al. 2015; Forman et al. 2017; Krzesinska and Almeida 2019), or micro- and nanostructural details of minerals (e.g., Hanna et al. 2015; Ruzicka et al. 2015; Ruzicka and Hugo 2018).

The aim of this study was to define mechanisms that operated in the formation of the texture of the ungrouped enstatite meteorite Zakłodzie. This meteorite has mineral and chemical compositions close to EL chondrites (Stępniewski et al. 2000; Przylibski et al. 2005), but it clearly has highly equilibrated, "achondritic-like" texture. Zakłodzie is a fine-grained rock. It predominantly consists of subhedral enstatite crystals, which reveal features of substantial recrystallization but also striation. In places, enstatite is set in interstitial, skeletal plagioclase and up to 20 vol% of opaque minerals may be present (Przylibski et al. 2005). Based on various mineralogical and chemical studies, it was proposed to represent either a primitive enstatite achondrite (Przylibski et al. 2005), an EL7 chondrite (Stępniewski et al. 2000), or an impact melt rock (Burbine et al. 2000; Keil 2007). In order to identify mechanisms and the sources of heat in petrogenesis of Zakłodzie, we performed fabric and texture analysis and combined it with a pyroxene TEM nanostructure study.

SAMPLES AND METHODS

The Zakłodzie meteorite was found in 1998 in Poland. It was one specimen with a mass of 8.68 kg, which later on was subsampled. Two cm-sized chips from the interior of Zakłodzie were scanned using high-resolution X-ray computed tomography (XCT) to characterize the general structure and fabric of opaque phases, Fe,Ni-metal, and troilite. The scanning was performed with the Nikon HMXST 225 System at the Natural History Museum in London, operating with a tungsten source that emits a polychromatic X-ray beam. Analytical conditions were set up to 190 kV voltage and 200 μA beam current to obtain optimum absorption contrast. A 0.5 mm thick Cu filter was placed between the X-ray source and sample to reduce beam hardening artefacts; 3142 projections were acquired during full 360° rotation scanning (at an angle of 0.114° per step) and recorded under static conditions to minimize ring artifacts. Two frames per projection were acquired and averaged. A modified Feldkamp back-projection algorithm (Feldkamp et al. 1984) was used to reconstruct the data. The effective voxel (i.e., three-dimensional pixel) size of the reconstruction is 6.7 μm.

Reconstructed tomographic data sets were used to infer a general structural characteristic of the meteorite and to quantify petrofabric parameters. Three-dimensional visualization and volume rendering were performed with free ImageJ® (Schneider et al. 2012) and Avizo software available at the NHM. Opaque phases (both metal and sulfides) were segmented based on gray level threshold using the Avizo software. During segmentation procedure, grains smaller than 10 voxels (~3 voxels in each dimension) were identified as potential noise and discarded from further statistical analysis. Segmented grains were approximated by best-fit ellipsoids with axes defined as $a \geq b \geq c$, and orientations for each best-fit ellipsoid were computed. Orientations (trend and plunge) of the major (a) axes of each individual best-fit ellipsoid were projected onto equal area stereonets in Stereo32 software.

Petrographic and textural analyses of the meteorite were obtained with optical microscopy and BSE imaging on four thin sections. SEM-BSE images were collected with an accelerating voltage of 8 keV and 1 nA current. Based on the collected images, the distribution of metal and sulfide grains was qualitatively described in ImageJ® (Schneider et al. 2012), with a particular emphasis on defining textural parameters such as length of metal-sulfide contacts and dihedral angles the sulfides have with silicates (Guignard and Toplis 2015; Barnes et al. 2017). These parameters were shown by Guignard and Toplis (2015) to correlate best with the advancement of metamorphic solid-state

recrystallization that defines the onset of primitive achondrites formation (an example of acapulcoites and lodranites). Length of metal-sulfide contacts was quantified according to the definition of Guignard and Toplis (2015), i.e., we digitally segmented the length of contacts of metal and sulfide grains and normalized it to the area the opaque minerals represent.

Based on the petrographic analysis, three electron-transparent foils for transmission electron microscopy (TEM) were extracted from striated enstatite crystals. Foils were prepared using site-specific focused ion beam (FIB) milling with a 30 kV Ga^+ ion beam at various currents. Sites for extraction were selected to best reveal pyroxene nanostructure along (100) crystallographic plane. The extracted foils of size 15–20 μm × 10–15 μm and of thickness ~100 nm were placed on a perforated carbon film on a copper grid and investigated in TEM.

The foils were studied by scanning transmission electron (STEM) imaging, followed by bright-field and high-resolution TEM analysis and selected area diffraction (SAED) patterns were collected from selected areas. The TEM used was a FEI Tecnai G2 F20 X-Twin at the GFZ Potsdam operated at 200 keV with a field emission gun as electron source.

RESULTS

Structure of the Meteorite in 3-D

Zakłodzie reveals heterogeneous structure in cm-scale when scanned tomographically in 3-D. Heterogeneity is manifested mainly by the distribution of metal and sulfides (Figs. 1A–C). Parts of the meteorite are rich in large, mm-sized irregular grains of metal and sulfide, called "lithology A." Other parts, denoted as "lithology B" (Fig. 1), are characterized by sulfides and metal smaller in size (100–400 μm) when compared to lithology A and more regular in shapes (Table 1). Sulfides and metal in the lithology B are intimately overgrown with silicates in a network-like pattern (Figs. 1D and 1E). Boundaries between the two lithologies appear indistinct, and no signs of brecciation were identified.

Petrographic Description and Quantification of Textural Parameters

The rock is composed predominantly of 0.1–1 mm enstatite, euhedral–subhedral in shape and striated parallel to the direction of elongation. The crystals are set in abundant Fe,Ni-metal, sulfides, and plagioclase that infill interstitial spaces. The nature and microtextures of interstitial spaces vary between the parts recognized as lithology A and B.

Lithology A contains abundant, millimeter-sized, twinned plagioclase crystals that poikilitically enclose enstatite. Multiple growth twins in plagioclase are aligned parallel and extinction orientation of the twins is coherent across whole plagioclase grains, i.e., up to millimeters, in agreement with poikilitic texture (Fig. 2). The largest plagioclase patches encapsulate metal and sulfides. Opaque minerals have lobate, irregular boundaries with plagioclase (Figs. 3A and 3B). Metal and sulfides co-occur in a form of overgrown assemblages. To quantify the degree of their separation, their contact length ratio (Guignard and Toplis 2015) was calculated, and is approximately 0.001 (Table 1).

Lithology B is characterized by less common or absent interstitial plagioclase. In these parts, opaque minerals form distinct separate grains of either Fe,Ni-metal or sulfide, at the contact with enstatite. Enstatite and opaque minerals are characterized by euhedral shapes and straight boundaries (Figs. 3C and 3D), with distinct triple junctions between enstatite, metal, and sulfides. Metal and sulfides are separated, and their contact length ratio is approximately 0.0002, an order of magnitude lower than for the lithology A (Table 1). Dihedral angles of sulfides with enstatite show a broad distribution range, from 30° to 130°, with a maximum at 60–80° and a weaker maximum at 110–120° (Fig. 4). Additionally, a thin film of metal/sulfide is observed along the enstatite contacts.

Fabric Analysis

The fabric was analyzed separately for each defined lithology. For this purpose, ~1500 grains of metal and sulfide were manually assigned in tomographic reconstructions to a specific lithology and then segmented. Segmented grains were approximated by best-fit ellipsoids and 3-D spatial orientations for each best-fit ellipsoid were computed and ploted in fixed spatial reference framework.

The petrofabric analysis shows distinctive differences between both lithologies. Metal and sulfide grains approximated by best-fits ellipsoids reveal preferred shape orientation of their longest axes (a axes) in both lithologies. However, the fabric geometry and orientation is not consistent through the meteorite (Fig. 5). In lithology A, the majority of grains have their longest axes aligned in a preferred direction or scattered along a great circle (Fig. 5A). This scatter defines fabric with foliation and also a strong lineation direction (Fig. 5C). In contrast, segmented grains in lithology B display only weak preference to be scattered along a great circle, i.e., only weak foliation is present (Figs. 5B and 5D). As seen already in the rough

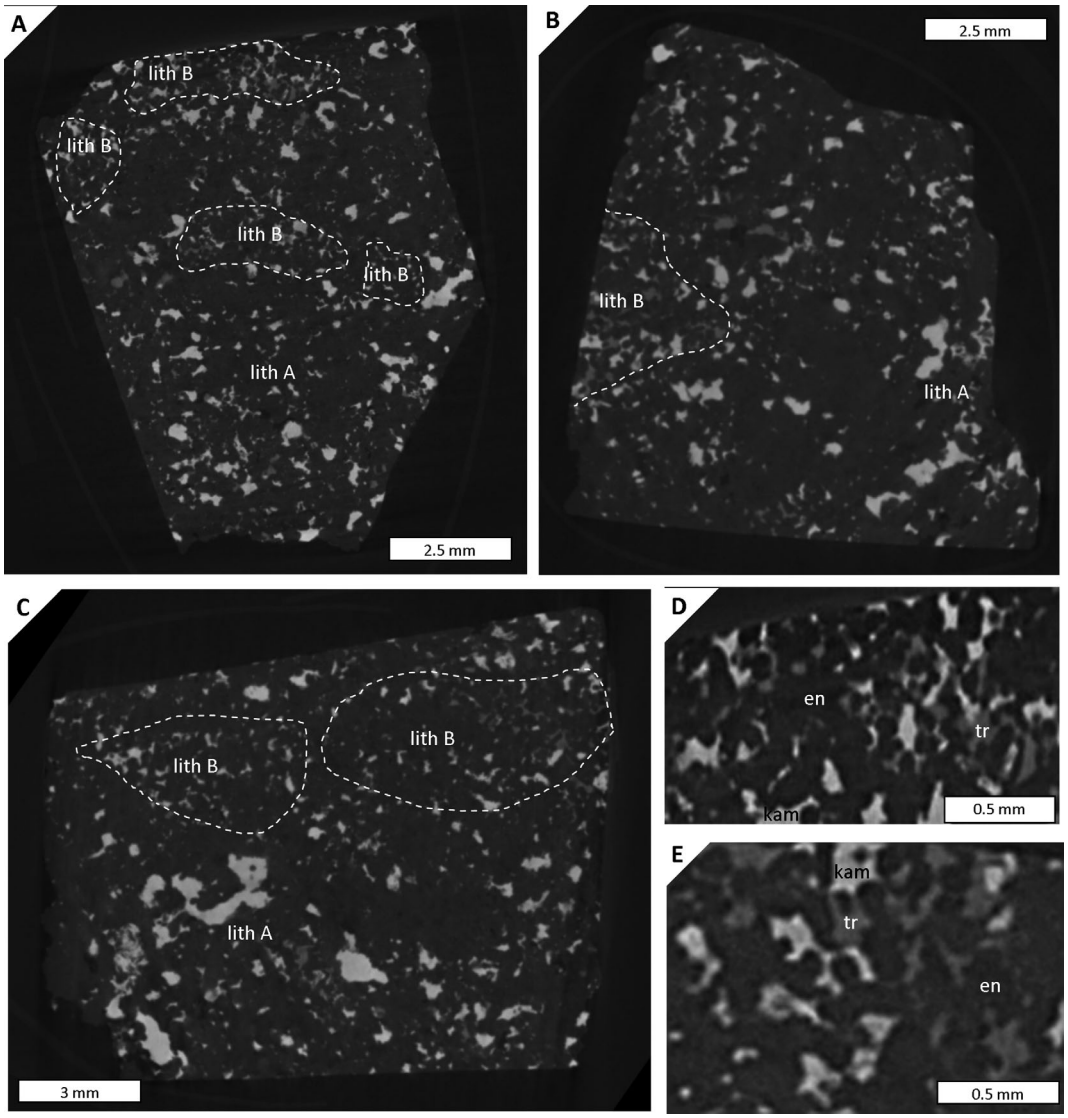

Fig. 1. Example X-ray computed-tomographic slices through Zakłodzie enstatite meteorite. Based on shapes, sizes, and textural features of metal (white) and sulfide (light gray) grains, two different lithologies may be distinguished. Lithology A (lith A) contains large, irregular grains of metal and sulfides, while the lithology B (lith B) is characterized by rather small grains that are more regular in shape and intimately overgrown with silicates (dark gray). The boundaries of the lithologies are indistinct, but the textural details of the grains are contrasting enough for the lithologies to be distinguished. A–C) Examples of tomographic slices through Zakłodzie. D, E) Enlarged view of opaques in parts assigned as lithology B. kam = FeNi-metal (kamacite), tr = troilite, en = enstatite.

tomographic images, opaque minerals in lithology B form an elongated, network-like structure (Figs. 1D and 1E). Aside from distinct differences in geometry of fabric, both lithologies differ also in fabric orientation (Table 1; Fig. 5) despite the same spatial framework was applied in reconstruction for both lithologies.

Keilite in Lithology A

In several cases, metal grains in lithology A are in contact with two separate sulfides, troilite (FeS) and keilite ((Fe,Mg,Mn)S), as seen in thin sections. The assemblages are also seen in tomographic reconstructions which allows visualizing their spatial relationship and distribution. Although XCT analysis is not quantitative in terms of the chemical composition of sulfides, by analogy to assemblages observed in the thin sections, the gray level scale contrast between the two sulfide phases in the XCT images (Figs. 6A and 6B) may be attributed to presence of lighter elements, Mg and Mn in keilite (darker in XCT) instead of heavier Fe in troilite (lighter in XCT). In 3-D reconstructions,

Table 1. Modal composition, median grain size, and parameters describing texture and fabric of mineral components in lithologies A and B in Zakłodzie.

	Modal composition (vol%)				Median grain size (μm)				
	En	Plag	Met	Sulf	En	Plag	Met	Tro	Ke
Lithology A	~75	10–12	10	6	100–800	up to 1500, twinned, skeletal crystals	200–1500, often up to 4 mm	100–500	200–500, up to 1 mm
Lithology B	~80	up to 4	6	5	100–1000	up to 200, interstitial	100–400	200–400	not seen

	Textural parameters		
	Metal-sulfide contact length [ratio; unitless]	Sulfide-silicate dihedral angles	Fabric of opaque phases
Lithology A	0.001	Grains encapsulated in plagioclase, no dihedral angle information	Weak foliation and lineation L = 50/45
Lithology B	0.0002	Predominantly 60–80°, minor 110–120°	Weakly defined foliation F = 120/80

En = enstatite; Plag = plagioclase; Met = Fe,Ni-metal; Sulf = all sulfides; Tro = troilite; Ke = keilite.

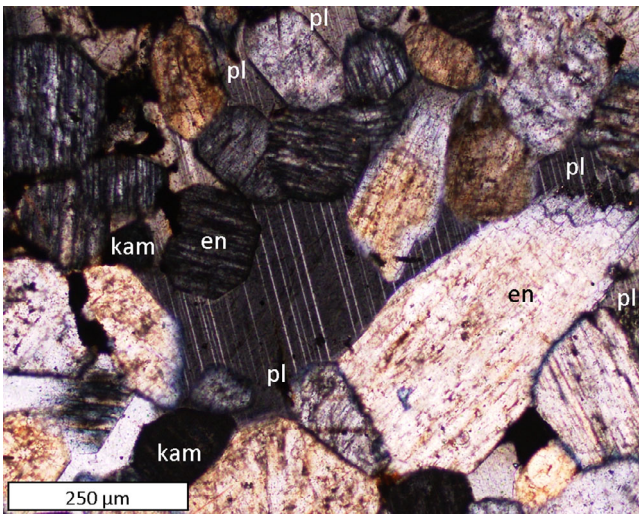

Fig. 2. Plagioclase in Zakłodzie lithology A. Multiple growth twins of plagioclase (pl) are aligned parallel across domains up to 1 mm in size. Plagioclase crystals poikilitically enclose enstatite (en) grains and encapsulate some metal (kam) and sulfide grains. Optical microphotograph, crossed polars. (Color figure can be viewed at wileyonlinelibrary.com.)

keilite in the assemblages always occurs at the contact of metal and troilite (Figs. 6C and 6D) and keilite is larger than 100 μm in size.

No keilite was found in the lithology B, neither in XCT scans nor in thin sections. Taking into account the resolution of XCT scanning (6.7 μm/voxel), this means that no keilite grains larger that 20–30 μm are present in the lithology B.

Nanostructure of Enstatite

Enstatite crystals in Zakłodzie are striated along their elongation direction, parallel to (100) plane. This is indicative of a mixture of both orthorhombic and monoclinic polymorphs which occur as intercalating lamellae of variable thickness (e.g., Iijima and Buseck 1975). To reveal nanostructural details of the striated crystals, the crystals were examined utilizing TEM. FIB foils for the study were extracted from the selected crystals in a way to examine both lithologies of Zakłodzie.

In striated crystals, clinoenstatite and orthoenstatite occur as alternating lamellae displaying lattice fringes with d-spacing of 1.8 and 0.9 nm in (100) plane (Fig. 7). Many partial dislocations associated with stacking faults are present (Figs. 7A–C).

In all studied foils, domains of clino- and orthoenstatite are heterogeneously distributed and are of highly variable width (Fig. 8). In some places, very thin lamellae of both orthorhombic and monoclinic enstatite are abundant, coherently intercalated with each other, and causing extreme streaking normal to the lamellae planes in electron diffraction patterns (Fig. 8A). The streaking in the electron diffraction is due to very thin platelets. In some other areas, the packages of clinoenstatite are up to 10 nm in width (i.e., ~10 unit cells) (Fig. 8B). However, the packages are also intergrown with thin, minor orthoenstatite domains.

In lithology B, a tendency of clinoenstatite to occur as the prevailing phase is observed. Although orthoenstatite still is present, it forms very thin lamellae, usually just one unit cell, very occasionally up to 10 nm wide. Clinoenstatite packages reach in this lithology up to 20 nm in thickness (Fig. 8C). In some parts of crystals, the packages of clinoenstatite are thicker (~40 nm), only minor streaking is visible in diffraction patterns, which is in accordance with the increased thickness (Fig. 8D).

Striated crystals are fractured. In many cracks, traces of healing are observed (Fig. 9). Cracks that cut

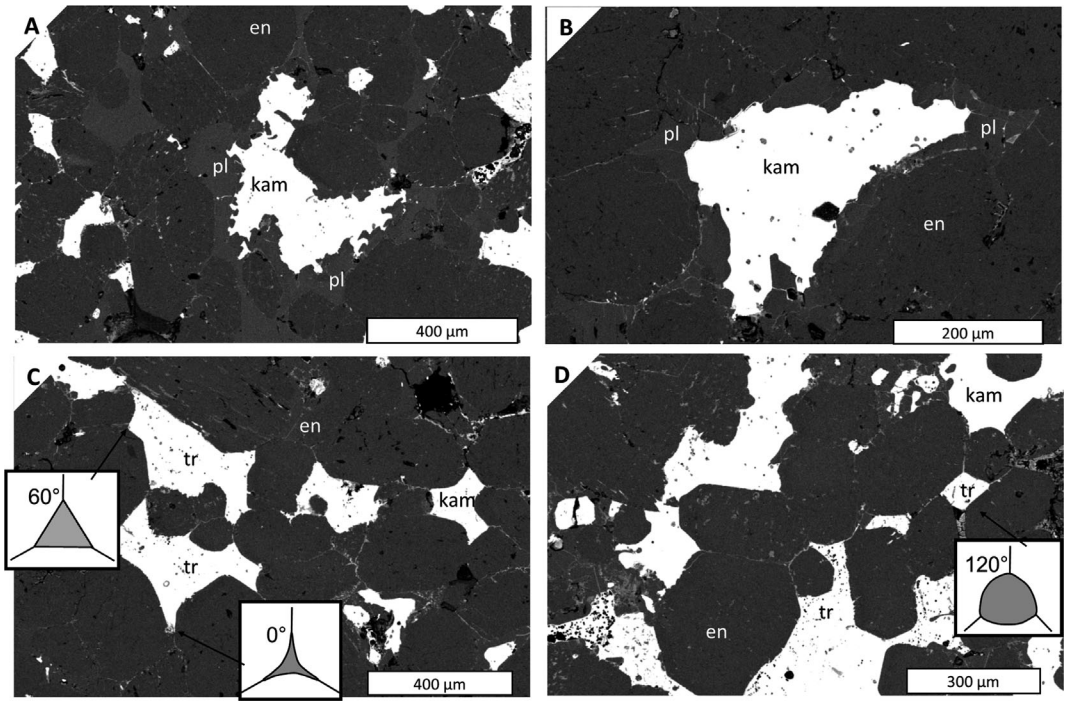

Fig. 3. Textural features of opaque phases and interstitial plagioclase in the two lithologies in Zakłodzie. BSE images. Typical dihedral angles of sulfides and enstatite are shown in inserts. A) In lithology A, FeNi-metal (kam) is associated with plagioclase network and it tends to form irregular grains, while sulfides are more euhedral and more separated. A significant amount of interstitial plagioclase (pl) occurs between enstatite (en). B) Irregular-shaped, lobate metal grain (kam) enclosed in interstitial plagioclase (pl). Lithology A. C) In lithology B, both kamacite (kam) and sulfides (tr) form euhedral grains interstitial to enstatite (en) and reveal triple junctions with silicates. D) Parts of the lithology B with sulfides (tr) separated from Fe,Ni-metal (kam). The lithology B is clearly depleted in plagioclase as compared to the lithology A.

through lamellae are partly or fully annealed and pyroxene crystallites visibly intrude into the open spaces in cracks (Figs. 9B and 9D). Some voids along the healed fractures are usually preserved (Figs. 9B and 9C). Material filling in the cracks is highly disordered or amorphous (Fig. 9E). The amorphous state is documented by diffuse scattering intensity in electron diffraction patterns. Near the annealed area clinopyroxene is a dominating phase.

DISCUSSION

The aim of our study was to identify the mechanisms and processes responsible for the textural evolution of Zakłodzie. When identified, these mechanisms serve as a base to address the question about processes involved in the petrogenesis of the meteorite.

Enstatite Nanostructure—Shock and Shearing-Induced Inversion

The intercalation of orthorhombic enstatite with monoclinic polymorphs, such as observed in striated crystals of Zakłodzie, may have formed by different mechanisms, which operated in very different temperature and pressure regimes. According to low-Ca pyroxene *P-T* phase diagrams (e.g., Presnall 1995; Jahn and Martoňák 2009; Fig. 10) enstatite may form three stable or metastable phases: protoenstatite, orthoenstatite, and clinoenstatite. Protoenstatite is stable only under high temperatures and during cooling, it inverts preferentially to orthoenstatite. The cooling rates required to equilibrium transition are very slow; therefore under more rapid cooling, protoenstatite inverts into a mixture of ortho- and clinoenstatite. Additionally, at temperatures below 500 °C orthoenstatite is unstable and may invert completely or in part into clinoenstatite. The reverse transition occurs if clinoenstatite is reheated and annealed above 500 °C (Reid and Cohen 1967; Boland 1974; Buseck and Iijima 1975; Coe and Kirby 1975; Iijima and Buseck 1975).

In a meteoritic rock, intergrowths of orthorhombic and monoclinic polymorphs may have formed by the following transformations during any of the static accretionary evolution and shock-related processes (Fig. 10)

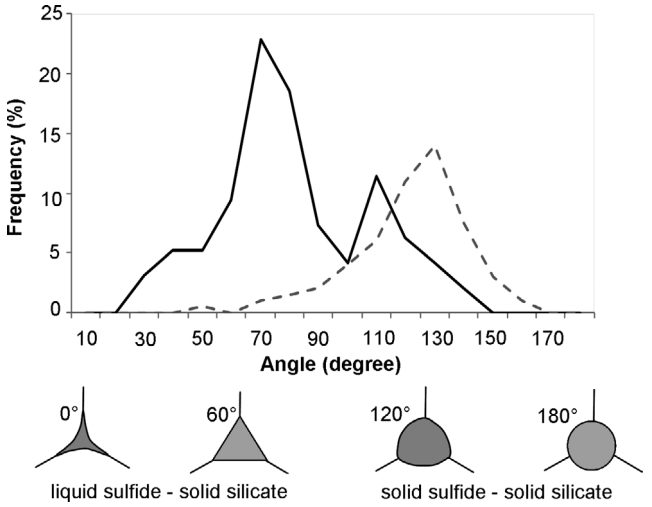

Fig. 4. Sulfide–silicate dihedral angle distribution in lithology B. Below the graph, representations of different dihedral angles between sulfides and silicates are shown (Sparks 1992). See Figs. 3C and 3D for examples of sulfides with respective dihedral angles with enstatite in Zakłodzie. The most frequent measured angles are in the range of 60–70°, consistent with solid silicate–liquid troilite equilibration textures (Barnes et al. 2017). Another smaller peak in distribution is present for the angles 110–120°. These are typical solid–solid dihedral angles, displayed by chondrites of high petrographic types (dashed line, after Guignard and Toplis 2015) and primitive achondrites such as acapulcoites and lodranites.

1. Relatively rapid cooling (quenching) of primary protoenstatite and simultaneous crystallization of both polymorphs (path 1 in Fig. 10; Buseck and Iijima 1975; Iijima and Buseck 1975). For the specific case of meteorites, this means crystallization of pyroxene from an igneous body and implies the presence of magma characteristic for achondrites (Keil et al. 1989).
2. Inversion of a monoclinic polymorph in orthoenstaite stability field (path 2 in Fig. 10; Buseck and Iijima 1975; Coe and Kirby 1975; Iijima and Buseck 1975), during a prograde metamorphic event, such as accretional metamorphism due to radiogenic heating associated by solid-state annealing (Brearley and Jones 1993).
3. Retrograde metamorphism associated with slow cooling. Such retrograde conditions may be obtained during static accretional metamorphism due to heating from the decay of radiogenic ^{26}Al (path 3 in Fig. 10; Brearley and Jones 1993) or by shock-induced heating if the rock, after a major impact event, was embedded in a warm ejecta blanket (Rubin 2004; Krzesinska and Almeida 2019).
4. Melting and rapid quenching in response to shock-related temperature increase (path 4 in Fig. 10; McCoy et al. 1995). This mechanism differs from the above mechanisms mainly in more rapid cooling rate and instantaneous quenching.
5. Heterogeneous, shock-related high strain-rate deformation, and mechanical inversion of orthorhombic structure into monoclinic polymorph, because monoclinic structure is more compatible with shearing (path 5 in Fig. 10; Coe and Kirby 1975; Iijima and Buseck 1975; Leroux et al. 1997).

Various studies utilized TEM analysis to identify the mechanisms responsible for the formation of striated mixture of enstatite in enstatite meteorites because orthorhombic to monoclinic transformation mechanisms are well reflected in the nanostructure. For example, Shallowater aubrite reveals enstatite crystals dominated by orthorhombic polymorphs (Keil 1989), which indicates the meteorite has crystallized from magma in an achondritic parent body (path 1 in Fig. 10). In TEM analysis, enstatite from Shallowater appears as a mixture of evenly distributed, thick domains of orthoenstatite with the presence of minor and thin clinoenstatite lamellae (Keil 1989). In contrast, Ilafegh 009 (Leroux et al. 1997) and Happy Canyon (McCoy et al. 1995) unclassified enstatite meteorites reveal in TEM analysis heterogeneously distributed, thin domains of ortho- and clinoenstatite. Such structure is interpreted as a result of quenching of shock-derived melt (path 4 in Fig. 10; McCoy et al. 1995; Leroux et al. 1997). Both annealing mechanisms (paths 2 and 3 in Fig. 10) cause coarsening of enstatite that is more stable under the respective pressure–temperature conditions. However, the distribution of the two polymorphs in crystals remains relatively even and homogeneous as the processes operate in static conditions (Buseck and Iijima 1975; Coe and Kirby 1975).

The nanostructure of enstatite in Zakłodzie, and highly heterogeneous distribution and variable thickness of ortho- and clinoenstatite domains, imply that the striated structure was attained in a dynamic process rather than by cooling and quenching. Electron diffraction patterns (Fig. 8) show strong streaking, indicative of a high degree of phase disequilibrium because the streaks are caused by presence of very thin lamellae of two phases. However, domination of clinopyroxene over orthopyroxene is observed (Figs. 7 and 8) and in general monoclinic pyroxene forms in places relatively broad domains (up to 40 nm in size i.e., they consist of more than 40 unit cells of cpx). On the contrary, the orthorhombic polymorph of pyroxene is minor, and it forms only very thin lamellae.

The only mechanism that may introduce such heterogeneity on the nanoscale level is shock-induced transformation, either quenching of shock melt or high strain-rate-related inversion (path 4 or 5 in Fig. 10). In Zakłodzie, highly striated grains show evidence of

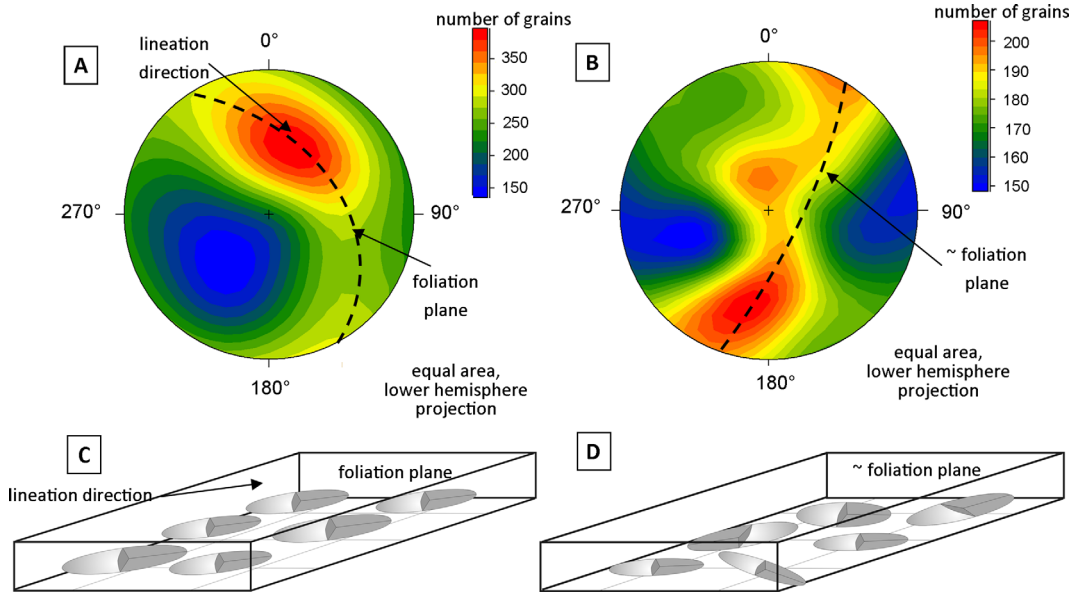

Fig. 5. Fabric of opaque grains (both metal and troilite) in the two lithologies in Zakłodzie. Orientation of the major axes of individual best-fit ellipsoids computed in fixed spatial reference framework and plotted on stereographic projections. A) Stereographic projection of major axes orientation of metal and sulfide grains segmented from lithology A. The projection shows well-developed fabric, with a weakly defined lineation direction. B) Stereographic projection of major axes orientation of metal and sulfide grains in lithology B. The graph shows that a weak fabric is developed only. Fabric orientation is not coherent with the fabric of the lithology A; therefore, it must have been significantly reprocessed or overprinted. C, D) The 3-D representations of the fabric elements in lithology A and B of Zakłodzie, respectively. For the lithology A, lineation component is clear, which means that major axes of the opaque grains (approximated by best-fit ellipsoids) show preferred orientation along a common direction. In the lithology B, the foliation plane is weakly defined, i.e., major axes of best-fit ellipsoids are scattered evenly in each direction and only fraction of them reveals preference to be oriented in a plane. Note that spatial orientation of fabric components in respect to an applied computational reference framework differs between lithologies A and B. Details on meteoritic fabric geometry and its computation from the high-resolution X-ray tomography (XCT) data sets are given elsewhere (Friedrich 2008; Friedrich et al. 2008; Krzesińska et al. 2015; Hanna and Ketcham 2017). (Color figure can be viewed at wile yonlinelibrary.com.)

stacking faults, dislocations, and kinking (Figs. 7B and 7C), which supports role of shearing and high strain-rate transformation. Additionally, the influence of shock-related shearing in the inversion of enstatite in Zakłodzie is consistent with the observed predominance of monoclinic polymorph, as this form is mechanically preferred under high strain rate conditions (Coe and Kirby 1975). Predominance of clinopyroxene domains in Zakłodzie is different from the nanostructure of enstatite form Happy Canyon and Ilafegh 009 (McCoy et al. 1995; Leroux et al. 1997) where domains of ortho- and clinopyroxene tend to occur in similar amounts.

Based on this observation, we argue that although enstatite from Zakłodzie was affected by a moderately strong shock event, it has never been shock-melted. Instead, enstatite was inverted by shock-related deformation in conditions below melting. This distinguishes Zakłodzie from Ilafegh 009 and Happy Canyon enstatite meteorites (McCoy et al. 1995; Leroux et al. 1997).

Pyroxene Postshock Annealing

The rapid shock event that affected Zakłodzie must have been followed by a mild thermal annealing period (path "Z" in Fig. 10). Such postshock annealing is required to account for completely and partly healed fractures in striated pyroxene (Fig. 9). Although the TEM results themselves do not provide a way to determine the temperature range of annealing, we argue (see discussion below) that it started above 500 °C, and continued during a slight temperature drop. The high-temperature stage possibly resulted in a minor secondary inversion of clino- into orthoenstatite, in accordance to *P-T* phase diagrams (Brearley and Jones 1993; Jahn and Martoňák 2009). This may account for local coarsening of orthoenstatite lamellae as is observed in TEM analysis (Figs. 7 and 8).

Lithology B is characterized by thicker domains of monoclinic enstatite and a minor amount of orthoenstatite in general (Figs. 8C and 8D). This is

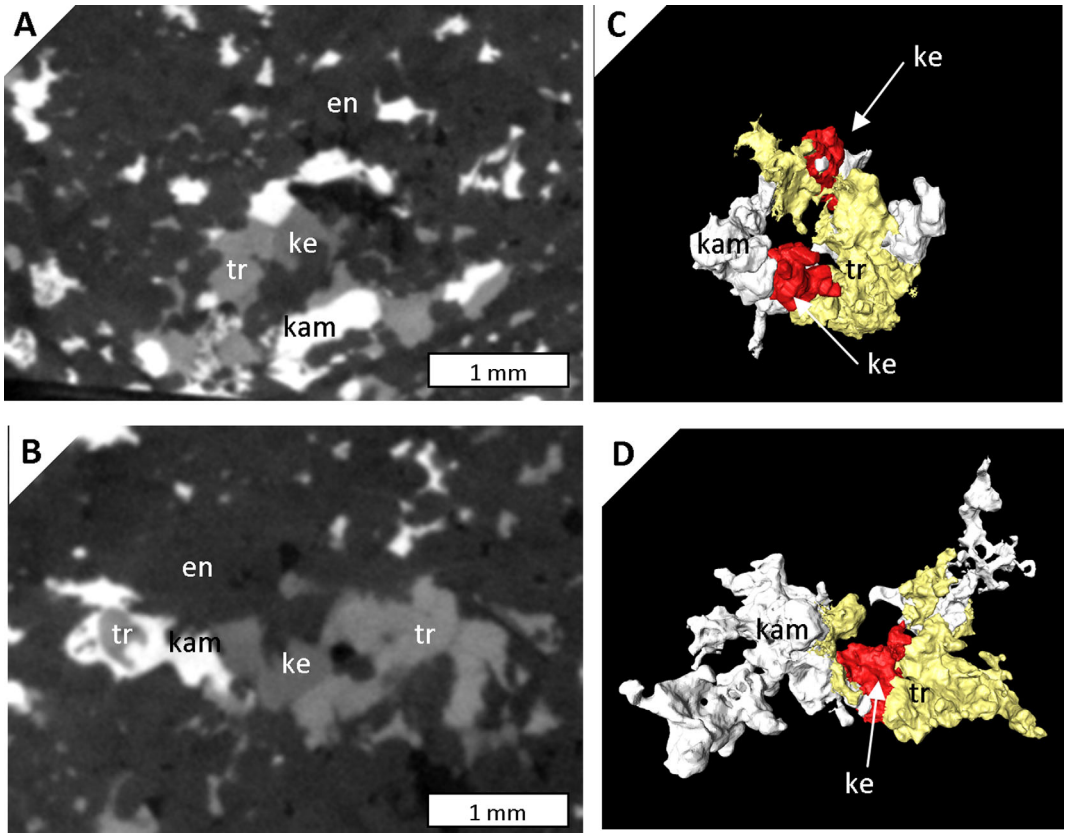

Fig. 6. Tomographic reconstructions of parts containing keilite in the lithology A. Due to a larger amount of light elements such as Mg, Mn, and Ca, keilite is darker than troilite (FeS) in XCT contrast. A, B) Cropped XCT images that show a textural relationship of metal (kam), troilite (tr), and keilite (ke). C, D) Three-dimensional segmentation of the phases shown in (A) and (B), respectively. Keilite is always present at the contacts of kamacite and troilite. (Color figure can be viewed at wileyonlinelibrary.com.)

interpreted to be a result of either stronger shock inversion or prolonged annealing in the field of clinoenstatite stability, i.e., below 500 °C (path "Z" in Fig. 10; see discussion below, as nanostructure exclusively does not provide a definite answer in this aspect).

Partial Melting

Plagioclase in lithology A poikilitically encloses enstatite crystals (Fig. 2). Multiple growth twins in plagioclase, continuing over several mm distances in sample indicate skeletal morphology of plagioclase that forms an interconnected network around enstatite crystals (McCoy et al. 1997). Metal and sulfide grains are connected to the plagioclase network and encapsulated in the plagioclase nodes (Figs. 2 and 3A–C). Such texture indicates that plagioclase and metal-sulfide crystallized from melt, while enstatite remained generally in solid state.

The texture of plagioclase and metal-sulfide is interpreted here as a result of the crystallization from partial melt, and we argue that partial melting occurred in equilibrium-based conditions (Tomkins 2009; Tait et al. 2014; Krzesińska 2016), as opposed to shock-based disequilibrium, incipient partial melting (Dodd and Jarosewich 1979; Krzesińska 2017). Although shock favors local melting of plagioclase and metal-sulfide, it is unlikely to be a driver for partial melting in Zakłodzie, based on lack of melt veins and pockets in this rock and taking into account large, mm-sized domains of plagioclase and metal-sulfide assemblages.

Although enstatite escaped from intense melting in Zakłodzie, it was perhaps affected by a minor partial melting. Przylibski et al. (2005) presented cathodoluminescence data suggestive that striated enstatite crystals possess secondary rims composed of clinoenstatite. This indicates that some enstatite was corroded and present in plagioclase-metal-dominated melt. During following crystallization from partial melt,

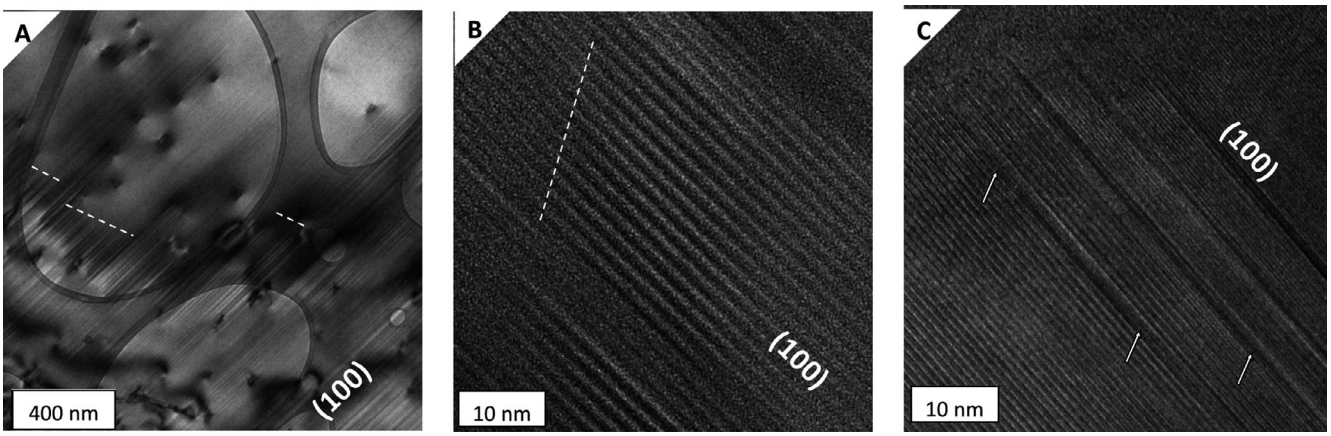

Fig. 7. General nanoscale overview of the structure of enstatite crystals in Zakłodzie. A) Bright-field TEM image showing pervasive striation of enstatite with lamellae developed parallel to (100). This is indicative of a mixture of two intergrown pyroxene phases. Stacking faults marked by dashed lines. B) High-resolution (HR) TEM image through striated area revealing intergrowths of both ortho- and clinoenstatite and additionally of stacking faults (dashed lines). C) HR-TEM image through a striated area. Alternating clinoenstatite and orthoenstatite lamellae are seen. Arrows indicate clinoenstatite that is discontinuous and terminates with stacking faults along partial dislocations.

monoclinic structure of pyroxene was favored because of low-temperature and low-pressure conditions (clinoenstatite stability field in Fig. 10).

The conditions of partial melting may be assessed based on results of laboratory experiments of partial melting in highly reduced conditions (McCoy et al. 1999; Fagan et al. 2000). The above experimental works concluded that partial melt with composition of plagioclase-metal/troilite plus minor enstatite reflects equilibrium partial melting at temperatures of ~1000 °C and up to 20% of volume of rock being involved in melting. It is important to note that such degree of partial melting under low oxygen fugacity is not associated with efficient melt segregation (McCoy et al. 1999).

Melt Segregation

Despite being partially molten, Zakłodzie does not record melt separation. The reason for the absence of extensive segregation may be a general feature of highly reduced partial melts (McCoy et al. 1997), where the melt is not removed. Additionally, the properties of troilite-metal-plagioclase melt are that the melt segregates in a limited way (Barnes et al. 2008, 2017). The two lithological parts in Zakłodzie differ in the amount of plagioclase, implying that locally, on a cm-scale, segregation occurred.

Our results show that metal encapsulated in plagioclase has a fabric with a lineation component (Fig. 5A). Lineation may reflect an influence of shearing, if metal was deformed in a solid state (Krzesińska et al. 2015). In Zakłodzie, such option may be excluded as the fabric is not coherent over the rock (Fig. 5A versus Fig. 5B), which means that the two lithologies were never deformed after partial melting. Additionally, lineated metal in Zakłodzie was clearly part of partial melt; therefore, the only possibility is that lineation determines the direction of flow of melt (Tait et al. 2014).

On the meteoritic parent body, flow of melt may be triggered by shock and local density-viscosity-driven segregation (Tomkins et al. 2013; Krzesińska 2017) or due to gravitational gradient, if the partially molten rock was located somewhere close to the surface of the body (gravitation gradient in the body center equals zero). In the case of Zakłodzie, partial melting clearly occurred under equilibrium conditions; therefore, shock may be excluded as a trigger. Therefore, lineation must reflect static parent body gradient features and location of the rock at some depth, but close to the surface of the asteroid.

Two-Phase Textural Equilibration During Cooling

Triple junctions between enstatite, metal, and sulfides, such as revealed in the lithology B of the Zakłodzie (Figs. 3C and 3D) indicate prolonged textural equilibration of the rock, which was obtained in retrograde metamorphism during slow cooling (path "Z" in Fig. 10). The textural and fabric parameters defined in our study reflect that cooling conditions in Zakłodzie were heterogeneous on the cm scale.

Dihedral angles of troilite with silicates in the lithology B indicate that first textural equilibration occurred between solid silicates and (liquid) sulfide melt. The most frequently measured dihedral angles in Zakłodzie are in a range of 60–80° (Fig. 3), which is consistent with equilibration of solid silicates with liquid

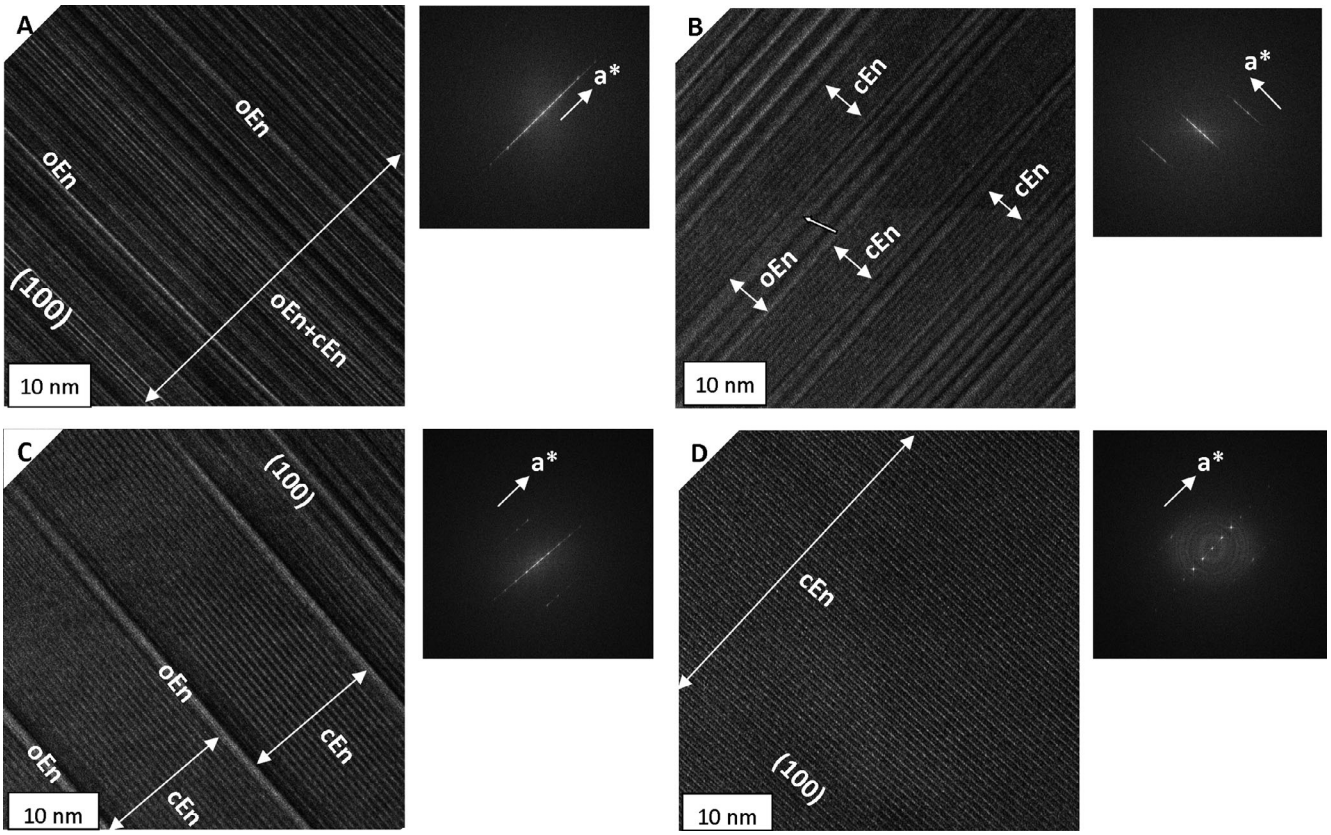

Fig. 8. High-resolution TEM images and selected area diffraction patterns (SADP) collected from striated enstatite crystals in the two lithologies in Zakłodzie. Lattice fringes with d-spacing of 0.9 and 1.8 nm in (100) plane indicate highly heterogeneous distribution of clinoenstatite (cEn, d-spacing of 0.9 nm) and orthoenstatite (oEn, d-spacing of 1.8 nm). A) Thin lamellae of clinoenstatite (0.9 nm) and orthoenstatite (1.8 nm) are intimately intergrown with each other. The diffraction pattern shows evidence of intensive streaking (diffraction patters in completely smeared) parallel to crystallographic a-axis, indicating that the lamellae are thin platelets. Lithology A. B) Irregular alternation of clinoenstatite and orthoenstatite. Lamellae of clinoenstatite form packages up to 10 nm in width and are intergrown with packages of orthoenstatite. Lithology A. C) Structure dominated by clinoenstatite, with lamellae that form packages up to 20 nm in thickness. Orthoenstatite lamellae are minor and thin, usually not larger than one unit cell. Lithology B. D) Package of clinoenstatite thicker than 100 nm. No streaking in a direction is observed in SADP (well defined diffraction spots). Lithology B.

troilite (Barnes et al. 2017). The shape of connected troilite grains and films between enstatite crystals (Figs. 1D, 1E and 3C, 3D) is consistent with such a process. We suggest that troilite was locally mobilized into silicates driven by wetting properties (Barnes et al. 2008, 2017). However, second minor peak in dihedral angles distribution is observed for values of 110–120° (Fig. 4). This suggests that second minor equilibration process operated in lithology B after the rock solidified, i.e., by diffusion between solid-state silicates and solid-state sulfides (Fig. 4) (Guignard and Toplis 2015).

The length of the contacts of metal and sulfides is another established proxy that reflects the advancement of textural equilibration in a solid state for equilibrated chondrites and primitive achondrites. It was shown by Guignard and Toplis (2015) that the reduction of the contact length is mainly attained by separation of sulfides from metal. They showed that, progressing from low petrographic, unequilibrated chondrites to type 6 chondrites, the phases become increasingly separated and suggested that separation occurs by solid-state diffusion. This trend is continued in primitive achondrites such as acapulcoites and lodranites. The degree of separation can be quantified using reduced normalized contact of the phases (Guignard and Toplis 2015). In Zakłodzie, metal-sulfide separation degree is different for grains assigned to lithology A and B. The contact length for lithology A is comparable with type 6 chondrites, while the lithology B reveals a significant separation of sulfides from metal, similar to primitive achondrites (Fig. 4). This means that the solid-state diffusion at low temperatures was relatively slow in the lithology B, while it was more rapid in the lithology A.

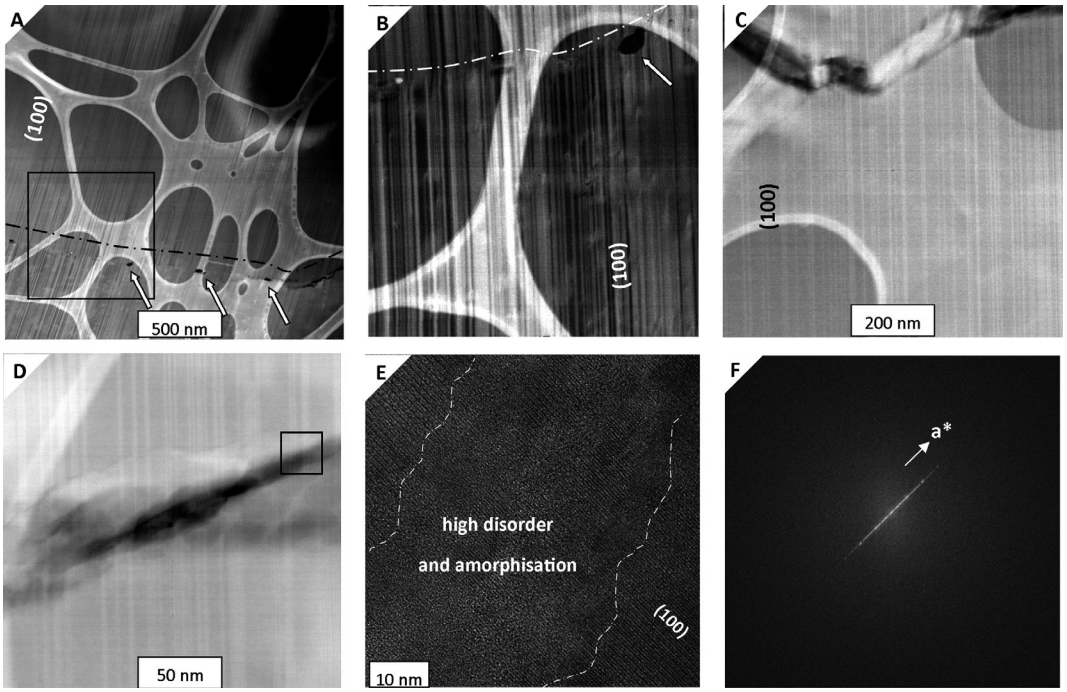

Fig. 9. Nanoscale markers of annealing of the enstatite in Zakłodzie. A) HAADF STEM image of striated pyroxene. Along a healed fracture (dashed line) enstatite lamellae are displaced. Fracture is partly annealed, retained holes are indicated by arrows. Web-like morphology appearing to be overprinted on lamellar structure is a contrast created due to the perforated carbon film the TEM foil rests on. B) The enlarged view of the rectangle marked in (A) to show annealing traces. An empty void in the fracture is indicated by an arrow. The enstatite lamellae along (100) are kinked in the healed fracture. C) STEM image of an annealed fracture. Crystallites grow into the crack but do not completely heal it. D) STEM image of partly annealed fracture. Crystals of pyroxene grow into the fracture at both sides. E) HR-TEM image of the area marked by the rectangle in Fig. 8D. Absence of lattice fringes or only weakly developed fringes in the area of an annealed crack indicates a high degree of disorder and/or amorphization. On both sides of the fracture, clinoenstatite occurs with lattice fringes of 0.9 nm d-spacing. F) SADP pattern collected for the disordered/amorphous part shown in Fig. 8E. Strong diffuse scattering intensity confirms disorder/amorphization of the material.

Indeed, another indication for rapid cooling at low temperatures in the lithology A comes from compositional zoning of plagioclase. Plagioclase in Zakłodzie reveals zonation of K and Na (Przylibski et al. 2005; Uribe et al. 2016). Additionally, some patches rich in K- and Si-rich glass and myrmecitic textures are present. Such textures in plagioclase form during localized rapid crystallization at temperatures below 500 °C.

Heterogeneous, Fast Cooling Below 500 °C and Partial Retention of Keilite

Keilite is a usual component of enstatite meteorites. Presence of sulfides of primarily lithophile metals such as Mn, Mg, Ca, Cr, and K is a general characteristic of enstatite meteorites and testifies to strongly reducing conditions (e.g., Keil 2007). It forms in a reaction of niningerite and alabandite with troilite, when both sulfides are heated above 500 °C and is stable in such temperature ranges. However, fast reaction rates in Fe-Mg-Mn-sulfides system facilitate back-reactions (Keil 2007). Consequently, no keilite can be retained if the system cools slowly.

In Zakłodzie, we observed keilite exclusively in association with metal and troilite in lithology A. No large keilite grains were identified by CT in other parts (taking into account the resolution of CT, grains larger than 20–30 μm are identifiable). Association of keilite with parts that were partially molten and cooled relatively quickly is consistent with its thermodynamic stability. Lack of keilite in lithology B may be interpreted as a proof for annealing of these parts. We suggest that keilite in these parts back-reacted and exsolved its FeS component due to slower annealing below 500 °C.

Although it is impossible to quantify cooling rates based on keilite, we expect that cooling in the lithology A was not rapid (not quenching). The composition of keilite in Zakłodzie, documented in details by Karwowski et al. (2007) is close to alabandite. We assume that keilite studied by Karwowski et al. (2007)

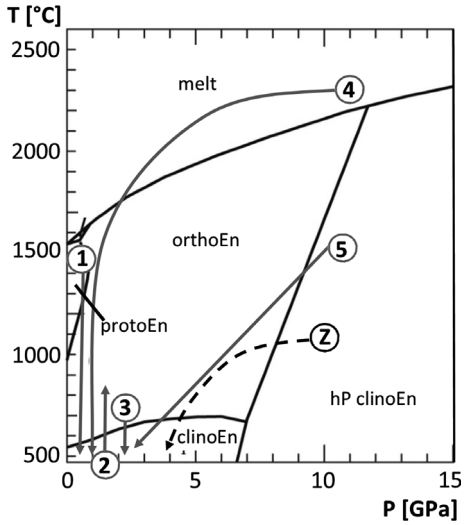

Fig. 10. Enstatite phase diagram with ortho- and clinoenstatite stability fields (after Presnall 1995). Arrows and numbers denote various scenarios and mechanisms that may lead to orthoenstatite–clinoenstatite transformations on meteoritic parent bodies. For details about the specific transformation scenarios, see the Enstatite Nanostructure—Shock and Shearing-Induced Inversion section. An inversion path proposed for Zakłodzie ("Z") is marked by dashed arrow and it involves shock transformation followed by mild annealing in ortho- and clinoenstatite stability field.

occurs in parts called here as lithology A. We interpret this as a sign of minor annealing that occurred in the sulfide system.

PETROGENESIS OF ZAKŁODZIE IN THE LIGHT OF IDENTIFIED MECHANISMS AND PROCESSES

Reconstruction of *P-T* Path and Identification of a Plausible Heat Source

Lithologies A and B in Zakłodzie record different degrees of partial melting and melt segregation, as well as different thermal and cooling histories. Lithology A experienced temperatures of metal-silicate partial melting and it cooled relatively slowly to 500 °C. At this stage shock-deformed pyroxene annealed (path "Z" in Fig. 10), keilite slightly equilibrated chemically toward alabandite and the texture equilibrated. However, below 500 °C cooling became faster, which accounts for a zonal composition of remnant plagioclase and for keilite generally being retained.

In contrast, lithology B must have cooled relatively slowly in both stages. This explains why it attained textural equilibrium in both stages, above 500 °C and below. Particularly, it accounts for pyroxene annealing in clinoenstatite stability field (path "Z" in Fig. 10) and for keilite to back-react. A long annealing period explains also why opaque phases in this lithology do not possess any fabric (Fig. 5B). The fabric of metal and troilite set in silicate matrix is easily obliterated while annealed (Friedrich et al. 2017).

Such a *P-T* path shows that cooling in Zakłodzie was not only a multiphase, complex process but also heterogeneous on the cm scale. Most plausibly, heterogeneous cooling was associated with postimpact conditions. The heating event in Zakłodzie clearly postdated the shock and brittle deformation. It is recorded in both pyroxene structure annealing (Fig. 9) and metal fabric (Fig. 5B). However, postshock heat itself is usually not sufficient to cause temperature raise large enough to initiate partial melting (Tomkins 2009; Tomkins et al. 2013). More important, cooling rates associated with postshock conditions are too fast (day to years scale) to lead to annealing and textural equilibration (e.g., Tomkins 2009). Therefore, we propose a more complex scenario involving impact to an already warm body. We suggest that the impact event provided instantaneous heat to commence melting, but the rock was already warm and capable to maintain cooling for a longer time.

Based on pyroxene nanometer scale deformation (Figs. 7 and 8), we conclude that the rock experienced a moderate shock event (S3–S4) that happened in the early evolution of the rock when the parent body was still warm due to internal radiogenic activity. Enstatite was inverted into a mixture of monoclinic and orthorhombic polymorphs, but not melted. Thermal energy released after shock from nearby regions was dissipated and added to the initial preshock temperature, which have caused a local increase of the temperature above 1000 °C. Because temperature increase occurred after the release of shock pressure, i.e., under static conditions, this process affected the larger volume of rock and moved toward thermal equilibrium. Thermal re-equilibration subsequently allowed the volume of rock to exceed the melting point and equilibrium-based partial melting commenced. At the stage when melting of troilite and metal started, melting reaction consumed some heat, therefore restrained further temperature increase (Mare et al. 2014). This started slow cooling and crystallization as well as facilitated annealing. Relatively slow cooling shows that the rock was insulated and heat dissipation took prolonged time during retrograde phase. Both lithologies in Zakłodzie differ so clearly in a record of thermal history and annealing on cm scale but their boundaries are very indistinct (Fig. 1). This is in a good agreement with contribution of postimpact heat dissipation to thermal budget.

Currently, enstatite achondrites and achondrite-like enstatite meteorites are considered as potential samples

derived from Mercury (McCubbin and McCoy 2016; Udry et al. 2019). Our study excludes such possibility, at least for Zakłodzie. Formation of texture in response to an early impact event to a warm body implies rather small size of the parent body.

Zakłodzie Petrogenesis and the Protolith Rock

Our study shows that Zakłodzie attained its texture due to an early impact event into a region of radiogenically heated enstatite chondrite/achondrite material located beneath the surface of the parent body. Due to insulation and the fact that the body was already warm, the postshock temperature equilibrated and remained above the solidus long enough for widespread equilibrium-based silicate-metal-sulfide partial melting, and for the melt to locally migrate. Alternatively, prolonged annealing may have occurred in a warm ejecta blanket (Rubin 2004), but such process would be reflected in a more complex fabric of opaque grains (Krzesinska and Almeida 2019), which is not observed in Zakłodzie.

Although Zakłodzie records influence of shock and impact, it cannot be considered as an impact melt rock or impact melt breccia (Burbine et al. 2000; Keil 2007; Keil and Bischoff 2008). Zakłodzie never experienced complete incipient impact melting. Instead, it was affected by equilibrium partial melting that operated under postimpact static conditions.

We argue also that Zakłodzie is neither an achondrite nor a residue after partial melting (Przylibski et al. 2005) as no signs for more extensive melting are found in texture. Textural features of Zakłodzie are indicators of the onset of partial melting and substantial recrystallization, characteristic for type 7 chondrites (Tait et al. 2014) and/or primitive achondrites (McCoy et al. 1997). We conclude that Zakłodzie represents a rock being texturally at the transition of chondrite–achondrite. The texture was obtained due to the contribution of early impact event(s) to the heat budget of the parent body.

However, it may still be debated whether the rock was chondritic or achondritic prior to shock. This question is still open and cannot be addressed with structural and textural analysis only. However, some former observations may be used to argue for chondritic parentage. Stępniewski et al. (2000) and Przylibski et al. (2005) observed clusters of enstatite that resembled chondrules and noted generally primitive chemistry of the rock. Also, noble gas signature was interpreted by Patzer et al. (2002) to be more alike to chondrites than achondrites. Additionally, Przylibski et al. (2005) mentioned relicts of forsterite in enstatite. Such relicts may be remnants of nebular reduction that affected enstatite chondrites (Herndon and Suess 1976; Weisberg et al. 1994). This agrees with our interpretation that enstatite crystals in Zakłodzie never underwent melting on the parent body, i.e., they represent still primordial chondritic crystals.

CONCLUSIONS

Three-dimensional petrofabric and texture analysis of the ungrouped enstatite meteorite Zakłodzie was combined with the nanostructural study of pyroxene to identify mechanisms leading to the formation of achondritic-like texture of the meteorite and to address the question of its petrogenesis.

Zakłodzie experienced a moderate shock event during its early evolution while being located at some depth of a warm parent body. Shock-related strain caused inversion of pyroxene to the mixture of intercalating orthorhombic and monoclinic polymorphs. The shock event was followed by a prolonged thermal event. The heat that dissipated after the shock pressure release was added to primary radiogenic-derived heat and caused local, equilibrium-based partial melting of plagioclase and metal-sulfide as well as a limited separation of melts. We estimate that up to 20% volume of rock was affected by partial melting and temperature reached up to 1000 °C. Partial melting was followed by two-stage cooling and retrograde annealing. The first phase of annealing (above 500 °C) allowed for crystallization of plagioclase and for textural equilibration of metal and sulfides with silicates. Below 500 °C, cooling was faster and heterogeneous over cm scale. It explains why Zakłodzie hosts keilite in some parts.

Based on our study, Zakłodzie is neither an impact melt rock nor a primitive achondrite. An impact melt origin is excluded because enstatite in Zakłodzie clearly has never been completely melted (although it was inverted by shock) and partial melting occurred during equilibrium-based postshock conditions and not during incipient phase of shock compression. Zakłodzie is not a primitive achondrite either, as it never experienced extensive melting due to internal activity on the parent body. Texturally, the rock represents a transition between chondrite and achondrite, but it owes its texture to the interaction of early impact heat and radiogenic-derived accretion heat.

Acknowledgments—The studied samples and thin sections come from the collection of Institute of Geological Sciences Polish Academy of Sciences. TEM analysis was conducted, thanks to the funding from European 7th Frame Program, RegPot (Research

Potential, ATLAB 285989). Meteoritical Society Travel Grant to A. M. K. allowed attending the 78th Annual MetSoc Meeting and discussion of results. A. M. K. acknowledges also support from The Research Council of Norway through its Centers of Excellence funding scheme, project number 223272. We thank Anja Schreiber (GFZ Potsdam) for preparation of FIB foils and Prof. Tadeusz Przylibski for discussion. This manuscript has benefited considerably from questions and comments of Alan Rubin and anonymous reviewer as well as from thorough editorial handling by Associate Editor Gretchen Benedix.

Editorial Handling—Dr. Gretchen Benedix

REFERENCES

Barnes S. J., Fiorentini M. L., Austin P., Gessner K., Hough R. M., and Squelch A. P. 2008. Three-dimensional morphology of magmatic sulfides sheds light on ore formation and sulfide melt migration. *Geology* 36:655–658.

Barnes S. J., Mungall J. E., Le Vaillant M., Godel B., Lesher C. M., Holwell D., Lightfoot P. C., Krivolutskaya A., and Wei B. 2017. Sulfide-silicate textures in magmatic Ni-Cu-PGE sulfide ore deposits: Disseminated and net-textured ores. *American Mineralogist* 102:473–506.

Boland J. N. 1974. Lamellar structures in low-calcium orthopyroxenes. *Contributions to Mineralogy and Petrology* 47:215–222.

Brearley A. J. and Jones R. H. 1993. Chondrite thermal histories from low-Ca pyroxene microstructures: Autometamorphism vs prograde metamorphism revisited (abstract). 24th Lunar and Planetary Science Conference. p. 185.

Brett R. and Keil K. 1986. Enstatite chondrites and enstatite achondrites (aubrites) were not derived from the same parent body. *Earth and Planetary Science Letters* 81:1–6.

Burbine T. H., McCoy T. J., and Dickinson T. L. 2000. Origin of plagioclase-"enriched," igneous enstatite meteorites. *Meteoritics & Planetary Science* 35:A36.

Buseck P. R. and Iijima S. 1975. High resolution electron microscopy of enstatite. II: Geological application. *American Mineralogist* 60:771–784.

Coe R. S. and Kirby S. H. 1975. The orthoenstatite to clinoenstatite transformation by shearing and reversion by annealing: Mechanism and potential applications. *Contributions to Mineralogy and Petrology* 52:29–55.

Dodd R. T. and Jarosewich E. J. 1979. Incipient melting in and shock classification of L chondrites. *Earth and Planetary Science Letters* 44:335–340.

Fagan T. J., Scott E. R. D., Keil K., Cooney T. F., and Sharma S. K. 2000. Formation of feldspathic and metallic melts by shock in enstatite chondrite Reckling Peak A80259. *Meteoritics & Planetary Science* 35:319–329.

Feldkamp L. A., Davis L. C., and Kress J. W. 1984. Practical cone-beam algorithm. *Journal of the Optical Society of America*. 1:612–619.

Forman L. V., Bland P. A., Timms N. E., Daly L., Benedix G., Trimby P. W., Collins G. S., and Davison T. M. 2017. Defining the mechanisms for compaction of the CV chondrite parent body. *Geology* 45:559–562.

Friedrich J. M. 2008. Quantitative methods for three-dimensional comparison and petrographic description of chondrites. *Computers & Geosciences* 34:1926–1935.

Friedrich J. M., Wignarajah D. P., Chaudhary S., Rivers M. L., Nehru C. E., and Ebel D. S. 2008. Three-dimensional petrography of metal phases in equilibrated L chondrites —effects of shock loading and dynamic compaction. *Earth and Planetary Science Letters* 275:172–180.

Friedrich J. M., Ruzicka A., Macke R. J., Thostenson J. O., Rudolph R. A., Rivers M. L., and Ebel D. S. 2017. Relationships among physical properties as indicators of high temperature deformation or post-shock thermal annealing in ordinary chondrites. *Geochimica et Cosmochimica Acta* 203:157–174.

Gattacceca J., Rochette P., Denise M., Consolmagno G., and Folco L. 2005. An impact origin for the foliation of chondrites. *Earth and Planetary Science Letters* 234:351–368.

Guignard J. and Toplis M. J. 2015. Textural properties of iron-rich phases in H ordinary chondrites and quantitative links to the degree of thermal metamorphism. *Geochimica et Cosmochimica Acta* 149:46–63.

Hanna R. D. and Ketcham R. A. 2017. X-ray computed tomography of planetary materials: A primer and review of recent studies. *Chemie der Erde—Geochemistry* 77: 547–572.

Hanna R. D., Ketcham R. A., Zolensky M., and Behr W. M. 2015. Impact-induced brittle deformation, porosity loss, and aqueous alteration in the Murchison CM chondrite. *Geochimica et Cosmochimica Acta* 171:256–282.

Herndon J. M. and Suess H. E. 1976. Can enstatite meteorites form from a nebula of solar composition. *Geochimica et Cosmochimica Acta* 40:395–399.

Iijima S. and Buseck P. R. 1975. High resolution electron microscopy of enstatite. I: Twinning, polymorphism, and polytypism. *American Mineralogist* 60:758–770.

Jahn S. and Martoňák R. 2009. Phase behavior of protoenstatite at high pressure studied by atomic simulations. *American Mineralogist* 94:950–956.

Karwowski Ł., Kryza R., and Przylibski T. A. 2007. New chemical and physical data on keilite from the Zakłodzie enstatite achondrite. *American Mineralogist* 92:204–209.

Keil K. 1989. Enstatite meteorites and their parent bodies. *Meteoritics* 24:195–208.

Keil K. 2007. Occurrence and origin of keilite, $(Fe_{>0.5}, Mg_{<0.5})S$, in enstatite chondrite impact-melt rocks and impact-melt breccias. *Chemie der Erde* 67:37–54.

Keil K. 2010. Enstatite achondrite meteorites (aubrites) and the histories of their asteroidal parent bodies. *Chemie der Erde* 70:295–317.

Keil K. and Bischoff A. 2008. Northwest Africa 2526: A partial melt residue of enstatite chondrite parentage. *Meteoritics & Planetary Science* 43:1233–1240.

Keil K., Ntaflos T., Taylor G. J., Brearley A. J., Newsom H. E., and Romig A. D. 1989. The Shallowater aubrite: Evidence for origin by planetesimal impacts. *Geochimica et Cosmochimica Acta* 53:3291–3307.

Krzesińska A. M. 2016. Thermal metamorphic evolution of the Pułtusk H chondirte breccia—Compositional and textural properties not included in petrological classification. *Geological Quarterly* 60:211–224.

Krzesińska A. 2017. Contribution of early impacts to metal-silicate separation, thermal annealing and volatile redistribution: Evidence in the Pułtusk H chondrite. *Meteoritics & Planetary Science* 52:2305–2321.

Krzesinska A. M. and Almeida N. V. 2019. Evidence of shock-induced vaporization of matrix to form porosity in Baszkówka, a porous L chondrite. *Meteoritics & Planetary Science* 54:54–71.

Krzesińska A., Gattacceca J., Friedrich J. M., and Rochette P. 2015. Impact-related non-coaxial deformation in the Pułtusk H chondrite inferred from petrofabric analysis. *Meteoritics & Planetary Science* 50:401–417.

Leroux H., Douckhan J. C., and Bischoff A. 1997. Mineralogy and crystallization history of the Ilafegh 009 EL-chondritic impact melt rock: An ATEM investigation. *Meteoritics & Planetary Science* 32:365–372.

Mare E. R., Tomkins A. G., and Godel B. M. 2014. Restriction of parent body heating by metal-troilite melting: Thermal models for the ordinary chondrites. *Meteoritics & Planetary Science* 49:636–651.

Mason B. 1966. The enstatite chondrites. *Geochimica et Cosmochimica Acta* 30:23–39.

McCoy T. J., Keil K., Bogard D. D., Garison D. H., Casanova I., Lindstrom M. M., Brearley A. J., Kehm K., Nichols R. H., and Hohenberg C. M. 1995. Origin and history of impact-melt rocks of enstatite chondrite parentage. *Geochimica et Cosmochimica Acta* 59:161–175.

McCoy T., Keil K., Muenow D. W., and Wilson L. 1997. Partial melting and melt migration in the acapulcoite-lodranite parent body. *Geochimica et Cosmochimica Acta* 61:639–650.

McCoy T., Dickinson T. L., and Lofgren G. E. 1999. Partial melting of Indarch (EH4) meteorite: A textural, chemical, and phase relations view of melting and melt migration. *Meteoritics & Planetary Science* 34:735–746.

McCubbin F. M. and McCoy T. J. 2016. Expected geochemical and mineralogical properties of meteorites from Mercury: Inferences from Messenger data (abstract #6242). 79th Annual Meeting of the Meteoritical Society.

Olsen E. J., Bunch T. E., Jarosewich E., Noonan A. F., and Huss G. I. 1977. Happy Canyon: A new type of enstatite achondrite. *Meteoritics* 12:109–123.

Passchier C. W. and Trouw R. A. J. 2005. *Microtectonics*. Berlin, Germany: Springer-Verlag.

Patzer A., Hill D. H., Boynton W. V., Franke L., Schultz L., Jull A. J. T., McHargue L. R., and Franchi I. A. 2002. Itqiy: A study of noble gases and oxygen isotopes including its terrestrial age and a comparison with Zakłodzie. *Meteoritics & Planetary Science* 37:823–833.

Presnall D. C. 1995. Phase diagrams of Earth-forming minerals. In *Mineral physics and crystallography: A handbook of physical constants*. AGU reference shelf 2, edited by Ahrens T. J. Washington, D.C.: American Geophysical Union. pp. 248–268.

Przylibski T. A., Zagożdżon P. P., Kryza R., and Pilski A. S. 2005. The Zakłodzie enstatite meteorite: Mineralogy, petrology, origin and classification. *Meteoritics & Planetary Science* 40:A185–A200.

Reid A. M. and Cohen A. J. 1967. Some characteristics of enstatite from enstatite achondrites. *Geochimica et Cosmochimica Acta* 31:661–672.

Rubin A. E. 2004. Postshock annealing and postannealing shock in equilibrated ordinary chondirtes: Implications for the thermal and shock histories of chondritic asteroids. *Geochimica et Cosmochimica Acta* 68:673–689.

Rubin A. E. and Scott E. R. D. 1997. Abee and related EH chondrite impact-melt breccias. *Geochimica et Cosmochimica Acta* 61:425–435.

Ruzicka A. M. and Hugo R. C. 2018. Electron backscatter diffraction (EBSD) study of seven heavily metamorphosed chondrites: Deformation systematics and variations in pre-shock temperature and post-shock annealing. *Geochimica et Cosmochimica Acta* 234:115–147.

Ruzicka A., Hugo R., and Hutson M. 2015. Deformation and thermal histories of ordinary chondrites: Evidence for post-deformation annealing and syn-metamorphic shock. *Geochimica et Cosmochimica Acta* 163:219–233.

Schneider C. A., Rasband W. S., and Eliceiri K. W. 2012. NIH Image to ImageJ: 25 years of image analysis. *Nature Methods* 9:671–675.

Sparks S. J. 1992. Magma generation in the Earth. In *Understanding the Earth—A synthesis*, edited by Brown G. C., Hawkesworth C. J., and Wilson R. C. L. Cambridge, UK: Cambridge University Press. pp. 91–114.

Stępniewski M., Borucki J., Durakiewicz T., Giro L., and Sharp Z. D. 2000. Preliminary study of a new enstatite meteorite from Zakłodzie (Southeast Poland). *Meteoritics & Planetary Science* 35:A152–A153.

Tait A. W., Tomkins A. G., Godel B. M., Wilson S. A., and Hasalova P. 2014. Investigation of the H7 ordinary chondrite, Watson 012: Implications for recognition and classification of Type 7 meteorites. *Geochimica et Cosmochimica Acta* 134:175–196.

Tomkins A. G. 2009. What metal-troilite textures can tell us about post-impact metamorphism in chondrite meteorites. *Meteoritics & Planetary Science* 44:1133–1149.

Tomkins A. G., Weinberg R. F., Schaefer B. F., and Langedam A. 2013. Disequilibrium melting and melt migration driven by impacts: Implications for rapid planetesimal core formation. *Geochimica et Cosmochimica Acta* 100:41–59.

Udry A., Wilburg Z. E., Rahib R. R., McCubbin F. M., Vander Kaaden K. E., McCoy T. J., Ziegler K., Bross J., Defelice C., Combs L., and Turrin B. D. 2019. Reclassification of four aubrites as enstatite chondrite impact melts: Potential geochemical analogs for Mercury. *Meteoritics & Planetary Science* 54:785–810. https://doi.org/10.1111/maps.13252

Uribe D. D., McCausland P. J. A., Izawa M. R. M., and Fleming R. L. 2016. A comparative study of the Zakłodzie and Northwest Africa 4301 anomalous enstatite achondrites (abstract #3071). 47th Lunar and Planetary Science Conference. CD-ROM.

Weisberg M. K., Prinz M., and Fogel R. A. 1994. The evolution of enstatite and chondrules in unequilibrated enstatite chondrites: Evidence from iron-rich pyroxene. *Meteoritics* 29:362–373.